Improvement of bit error rate and page alignment in the holographic data storage system by using the structural similarity method

Yu-Ta Chen,[1] Mang Ou-Yang,[2,*] and Cheng-Chung Lee[1]

[1]Department of Optics and Photonics, National Central University, Jhongli City 32001, Taiwan

[2]Department of Electrical Engineering, National Chiao-Tung University, Hsinchu City 30010, Taiwan

*Corresponding author: oym@mail.nctu.edu.tw

Received 7 March 2012; accepted 19 March 2012;
posted 22 March 2012 (Doc. ID 164331); published 1 June 2012

Although widely recognized as a promising candidate for the next generation of data storage devices, holographic data storage systems (HDSS) incur adverse effects such as noise, misalignment, and aberration. Therefore, based on the structural similarity (SSIM) concept, this work presents a more accurate locating approach than the gray level weighting method (GLWM). Three case studies demonstrate the effectiveness of the proposed approach. Case 1 focuses on achieving a high performance of a Fourier lens in HDSS, Cases 2 and 3 replace the Fourier lens with a normal lens to decrease the quality of the HDSS, and Case 3 demonstrates the feasibility of a defocus system in the worst-case scenario. Moreover, the bit error rate (BER) is evaluated in several average matrices extended from the located position. Experimental results demonstrate that the proposed SSIM method renders a more accurate centering and a lower BER, lower BER of 2 dB than those of the GLWM in Cases 1 and 2, and BER of 1.5 dB in Case 3.

OCIS codes: 210.0210, 210.2860, 210.1635.

1. Introduction

As a page-oriented storage approach [1], holographic data storage (HDS) is characterized by its high speed and large capacity [2–4] in contrast with conventional storage devices such as a digital video disk. Due to a rapidly increasing number of videos, pictures, music, games, and programs stored in a personal computer, the burgeoning demand for a large external storage capacity makes HDS a preferred alternative to hard disk drive (HDD) as a data backup device.

The HDS is constructed of a laser, spatial light modulator (SLM), storage material, image sensor, and optical components. The data are turned into gratings and then stored as two beams interfere with each other creating storage material. The data stored are then recovered from diffractive images sensed by an image sensor while the light inserts into the storage material. Distorted in the HDS system (HDSS) by various effects such as aberration, scattering [5], misalignment [6–7], and interpixel/page interference (IPI) [8–10], the distorted diffractive image also degrades BER and a signal-to-noise ratio (SNR) in HDSS. Among the several procedures developed to reduce the impact on HDSS include an oversampling method that reduces the misalignment and distortion effect [11], as well as a postprocessing method that repairs the pixel misregistration. It then reduces the blur effect on the images [6]. Our previous work developed the GLWM to discover the fiducial

1559-128X/12/163660-10$15.00/0

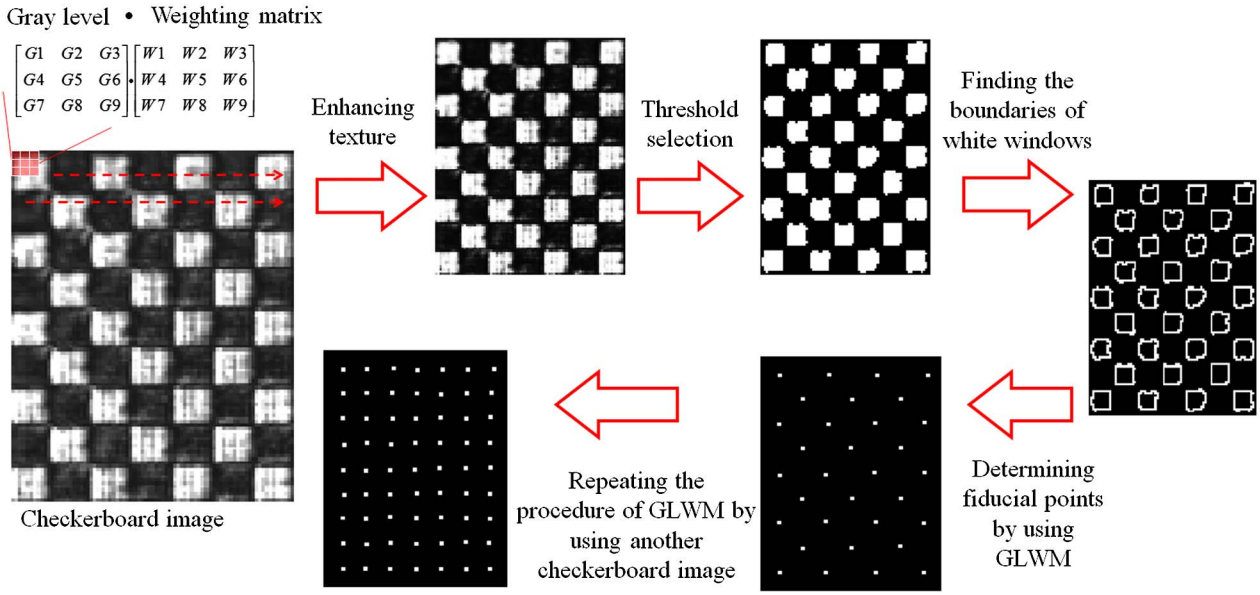

Fig. 1. (Color online) Procedure of fiducial points identifying with GLWM.

points on the received images for alignment, findings of which indicate that BER depends on the accuracy of the fiducial point position [12].

This work describes a structural similarity (SSIM) method to handle the alignment issue with checkerboard patterns, enabling HDSS to achieve a satisfactory BER while only requiring lower quality optical components or a loose mechanical tolerance. The advantages of SSIM over GLWM under various system conditions are described in detail.

2. Methodology

GLWM, an alignment method, identifies the fiducial point from the white windows of checkerboard images (Fig. 1) [12]. A swept weighting matrix is applied to two checkerboard images in order to obtain two new images of enhanced texture. Following threshold selection, both of the new images are transformed into the binary images and, then, the position of the boundaries between the white and the black windows in the binary images is determined using the boundary identification method. Finally, the position of the fiducial point is determined by averaging the positions of the white window boundaries. Theoretically, the block, surrounded by the black pixels or windows, should be fitted for the white window.

Owing to an inappropriate choice of the threshold level, a window contains two blocks (Fig. 2), while the window boundary is identified by GLWM. If a window contains more than one block, several fiducial points could be determined in a window, none of the fiducial points regarded as the window center correctly even determining the center of the fiducial points. Therefore, an image comparison algorithm, i.e., Pearson's correlation method, can replace thresholding and boundary searching. The image comparison is using a reference image (noise-free) to determine the position of the maximum similarity in the distorted image.

Prone to effects caused by thermal, scattering, and speckle noises, HDSS suffers from a significantly degraded image in terms of contrast, luminance, and structure. There are two issues in the image comparison of Pearson's correlation method. First, two identical images compared to each other causes the result into the form of 0/0. Second stronger noise exists between the white windows in the checkerboard image after the database matrices of smaller windows sweep over the checkerboard image. Accordingly, the image comparison approach is implemented using the SSIM method, i.e., an algorithm featuring a human vision. Implementation of SSIM method uses a reference image to comare locally with the distorted image by using a predistortion technique, i.e., a convoluted weight matrix with Gaussian distribution. The locally compared is that a square window moves

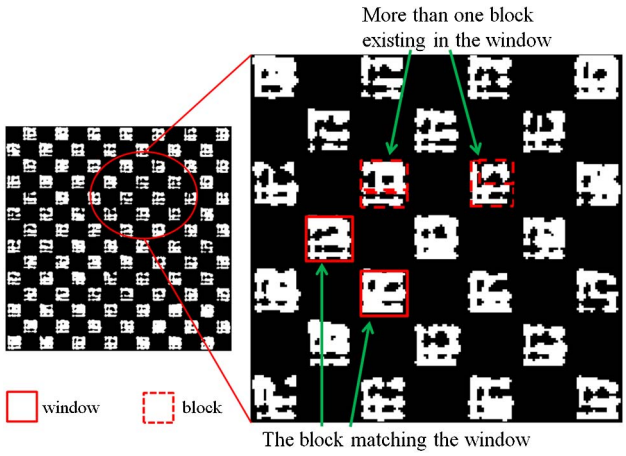

Fig. 2. (Color online) Fiducial points identifying with GLWM.

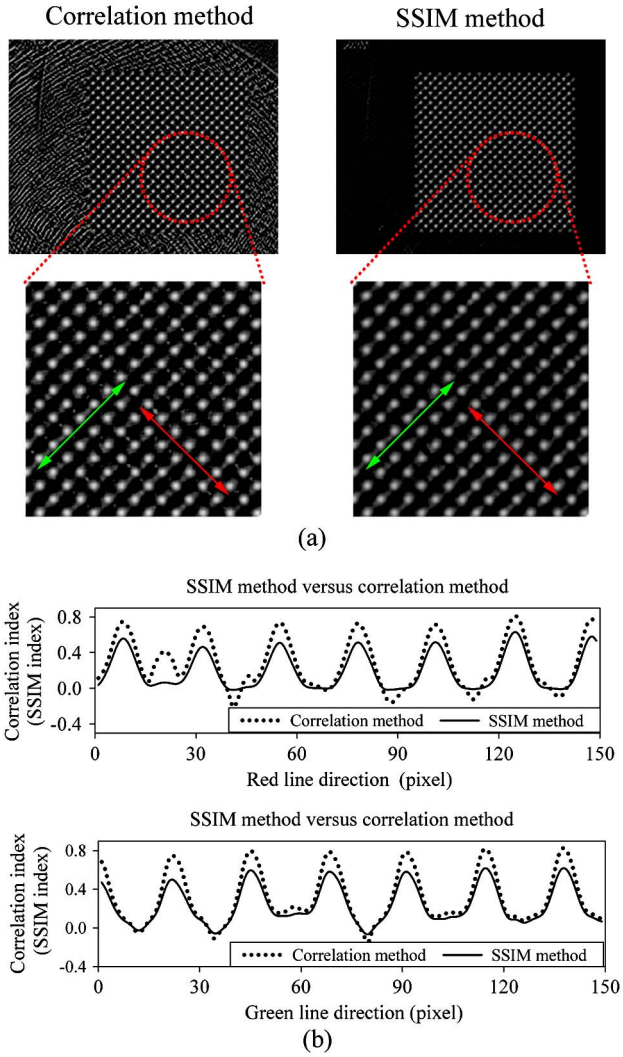

Fig. 3. (Color online) Plots of the comparison between Pearson's correlation method and SSIM method. (a) Swept checkerboard image comparison. (b) Comparison of correlation index in Pearson's correlation method and SSIM method.

pixel-by-pixel from the top left to the bottom right on the reference and distorted image. For each move determining, a SSIM index is determined from the comparison of the two images and all collected SSIM indices are averaged into a mean value. The mean SSIM index can describe the similarity degree between two images, therefore, extending the concept into page alignment. A reference image is used to sweep over the distorted checkerboard image of larger size and then, the fiducial points are identified as the mean SSIM index in the local maximum. Hereinafter, the SSIM index is equivalent to the mean SSIM index.

In Fig. 3(a), the swept checkerboard images are determined by using the SSIM method and the correlation method during the above processing, respectively, and the cropped image is from the equivalent position of the swept image. The correlation index (or SSIM index), −1 to 1, constructs the swept checkerboard image and is also corresponding to the gray level in the swept checkerboard image of Fig. 3(a), too. Owing to none of the stronger noise existing between the regions, which have the fiducial points, the cropped image of the SSIM method is clearer than the image of the correlation method. Figure 3(b) illustrates the distributions of the correlation index in the red and green lines of the cropped images. The stronger noise exists between the two peaks in the red line direction using the correlation method. In the green line direction of Fig. 3(b), the peaks of the correlation method are higher than the peaks of the SSIM method, but the peaks of the SSIM method still have local maximum to identify the fiducial points as weaker noise existing. Consequently, the SSIM method is suited to be used in the identification of the fiducial points in the HDSS.

Wang *et al.* [13] developed the SSIM formula, which takes into account three factors, i.e., luminance, contrast, and structure. Each factor is defined as a function and combined into the SSIM formula [13]. Applying this formula to image quality matrices can be expressed as

$$\mathrm{SSIM}(r,t) = \frac{(2\mu_r\mu_t + C_1)}{(\mu_r^2 + \mu_t^2 + C_1)} \times \frac{(2\sigma_{\mathrm{rt}} + C_2)}{(\sigma_r^2 + \sigma_t^2 + C_2)}, \quad (1)$$

where the subscripts r and t denote the reference and distorted images; μ_r and μ_t represent the mean values of r and t; σ_r^2 and σ_t^2 refer to the variance; σ_{rt} is the covariance between both images; and C_1 and C_2 denote both two small constants used to adjust the ratio between the preceding coefficients.

As an objective measure between two images, i.e., the reference and the distorted alike, the SSIM index ranges from −1 to 1 [13], according to the noise types and levels. A SSIM index of 1 implies that the two images are identical. However, for a SSIM index of −1, the two images are opposite in the luminance, contrast, or structure [14]. In this work, by using a checkerboard image and the SSIM method, the fiducial points are located as follows:

I. Construct two database matrices (images) of size 2×2 bits, alternate in black and white (Fig. 4).
II. The pixel number, covered by each bit in the database matrix, is exactly half of that, covered by

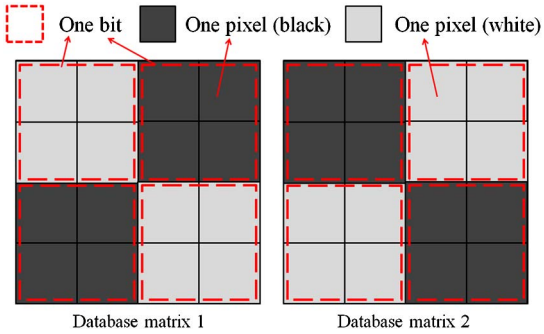

Fig. 4. (Color online) Sample of database matrices.

each bit on the checkerboard image, sensed from the image sensor.

III. The gray levels corresponding to black and white windows of the database matrices can be determined by the SNR of HDSS. (Default values of black and white windows are 0 and 255, respectively.)

IV. An identical size of the received checkerboard image to that of the database matrix is extracted, during which a SSIM operation is performed.

V. While sweeping over the received checkerboard image(s) by the database matrices, in each move receives a SSIM index, new images are thus constructed with the SSIM indices.

VI. Use a newly generated two-dimensional matrix to sweep over the new images and identify the local maximum of SSIM indices, aggregated as the so-called fiducial points.

The database matrix is equivalent to a reference image, a nondistortion and non-noisy image, which is used to identify the similarity structure in the checkerboard images by sweeping. Size of the database matrix is determined by the checkerboard image received by HDSS, given the system magnification and the number of pixels associated with each bit in the input image.

For instance, according to Fig. 5, each white and black window of the checkerboard images received from HDSS has approximately 5×5 pixels. Therefore, the size of the database matrix is set to 6×6 pixels, and the white and black windows of the database matrix are arranged as shown in Fig. 4. The swept database matrix, database matrix 1, starts from the top left portion of the checkerboard image, with each shifting receiving a new SSIM index; in addition, the local maximum of SSIM index likely occurs in position 2 in Fig. 5. After the database matrix sweeping over the checkerboard image, all SSIM indices are collected into a new image, as shown in Fig. 6 (top). The square windows are transformed into circle regions, and the distributions of SSIM indices are smooth and continuous in the regions (which surround the fiducial points). In the edge effect in the

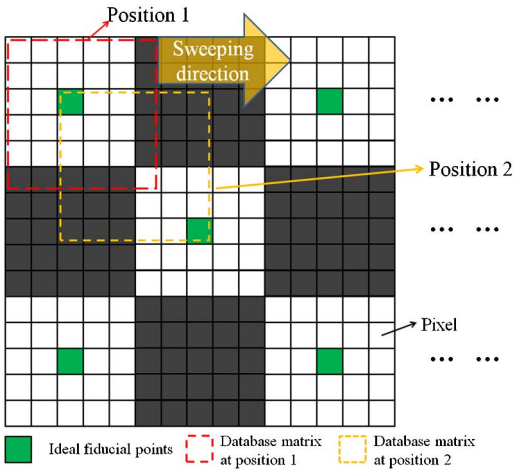

Fig. 5. (Color online) Example of fiducial points identifying with SSIM method.

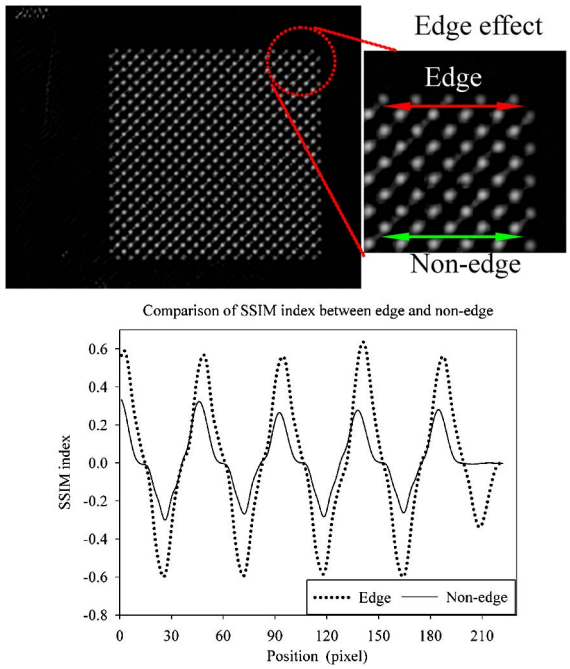

Fig. 6. (Color online) Edge effect in swept checkerboard image by using SSIM method.

edge regions of Fig. 6, the indices are lower than other regions since the database matrix cannot fully compare with the checkerboard image. Figure 6 (bottom) displays the comparison of SSIM indices between edge and nonedge. Restated, only half of the database matrix can compare with the edge of the checkerboard image, while the other half of the database matrix is out of the checkerboard image. Finally, a new matrix of 7×7 pixels sweeping over the new image discovers the fiducial points, while the local maximum of the SSIM indices is at the center of the new swept matrix.

The locations, numbers, and accuracy of fiducial points are affected by the values of C_1 and C_2 in the SSIM formula, the size of the database matrix, gray level threshold, and the matrix size in search of the maximum value. For a high SNR system, the system parameter tolerance negligibly influences the determination of the fiducial points. Conversely, a system with a low SNR exhibits a significant dependence of fiducial point locations on the parameter accuracy.

Before the BER calculation, a decided threshold must divide the gray level of the received images into 0 and 1. The BER can be defined as

$$\mathrm{BER} = p_0 \times p(1|0) + p_1 \times p(0|1), \tag{2}$$

where p_0 and p_1 denote probabilities that the total number is 1 or 0, respectively, $p(1|0)$ and $p(1|0)$ probabilities for 1 or 0 to be judged 0 or 1, respectively.

The SNR can also be expressed as [5]

$$\mathrm{SNR} = \frac{\mu_0 + \mu_1}{(\sigma_0^2 + \sigma_1^2)^{1/2}}, \tag{3}$$

where μ_0 and μ_1 denote the mean values of 0 and 1, and σ_0^2 and σ_1^2 denote the variance of 0 and 1, respectively.

In the SSIM operation starting, the database matrix is distorted to compensate for the noise of the distorted image by convoluting a weighting matrix with Gaussian distribution. In the right part of Eq. (1), σ_{rt}, σ_r, and σ_t dominate the value ranges of the right part of Eq. (1) from −1 to 1, and the sign of the value is determined by the sign of σ_{rt}. For explaining the predistorted database matrix compensating the distorted image, the variance and covariance are rewritten as follows:

$$\begin{aligned}\sigma_t^2 &= [a_{t0}(\sigma_{t0}^2+\mu_{t0}^2)+a_{t1}(\sigma_{t1}^2+\mu_{t1}^2)]-[a_{t0}\mu_{t0}+a_{t1}\mu_{t1}]^2\\ &= a_{t0}(\sigma_{t0}^2+\mu_{t0}^2-a_{t0}\mu_{t0}^2)+a_{t1}(\sigma_{t1}^2+\mu_{t1}^2-a_{t1}\mu_{t1}^2)\\ &\quad -2a_{t0}\mu_{t0}a_{t1}\mu_{t1}, \end{aligned} \tag{4}$$

$$\begin{aligned}\sigma_r^2 &= a_{r0}(\sigma_{r0}^2+\mu_{r0}^2-a_{r0}\mu_{r0}^2)+a_{r1}(\sigma_{r1}^2+\mu_{r1}^2-a_{r1}\mu_{r1}^2)\\ &\quad -2a_{r0}\mu_{r0}a_{r1}\mu_{r1}, \end{aligned} \tag{5}$$

$$\begin{aligned}\sigma_{\mathrm{rt}} &= \frac{1}{(N-1)}\sum_{x,y=1}^{N}(\mathrm{Gray}_r(x,y)-\mu_r)\times(\mathrm{Gray}_t(x,y)-\mu_t)\\ &= \frac{1}{(N-1)}\sum_{x,y=1}^{N}\mathrm{Gray}_r(x,y)\times\mathrm{Gray}_t(x,y)-N\mu_r\mu_t, \end{aligned} \tag{6}$$

where a_{t0} and a_{t1} denote the proportion of 0 and 1 to the total numbers in the distorted image; a_{r0} and a_{r1} denote the proportion of 0 and 1 to the total numbers in the database matrix.

According to Eq. (6), the covariance σ_{rt} varies with the gray levels of each pixel and the mean values in both images so that the distributions of the gray level in both images influence the degree of the covariance. However, the range of the right part of Eq. (1) can be determined as the hypothesized covariance. When the database matrix does not become distorted by convoluting Gaussian matrix, a_r is equivalent to zero and the value of the right part of Eq. (1) is dominated by the σ_t. As the database matrix is distorted by convoluting Gaussian matrix, σ_{rt} equivalent to σ_r^2 or σ_t^2, the value of the right part of Eq. (1) is determined as 1. Therefore, the value range of the right part of Eq. (1) is determined as $1/\sigma_t^2$ to 1.

The distribution of the distorted image is supposed to approach Gaussian distribution after Gaussian matrix convoluting in the SSIM operation and the database matrix are also convoluted Gaussian matrix to be distorted, too. However, the database matrix and the distorted image can be created by using Gaussian distribution approaching with different standard deviation and then the value of right part of Eq. (1) can be determined in varying standard deviations of both images. Figure 7(a) displays the standard deviations of the database matrix and the distorted image versus the determined value of right part of Eq. (1) as the mean values of both images fixed in each standard deviation. The solid line demonstrates the varying standard deviations of the distorted image, the standard deviation of 2.7 in the database image, and the maximal determined value occurs in the standard deviations of both images equalizing to each other. The dash line illustrates the varying standard deviations of the database matrix versus determined value of the left part of Eq. (1) as the standard deviation of 6 in the distorted image. Before the Gaussian matrix convoluting, the standard deviation of the database matrix equalizing to 0, the determined value is less than 0.1 in all cases. The slope in the left side of the maximal determined value is steeper than the right side one, and consequently, the noise tolerance can increase by using the predistortion technique in the SSIM operation starting. In the left part of Eq. (1), the relation between mean value of both images and the determined value is also solved and presented in Fig. 7(b). There are three mean value conditions, 50, 128, and 254, of the database matrix to show the direction of the determined value changing. The slope direction of the left part is similar to the case of the right part and SSIM value can

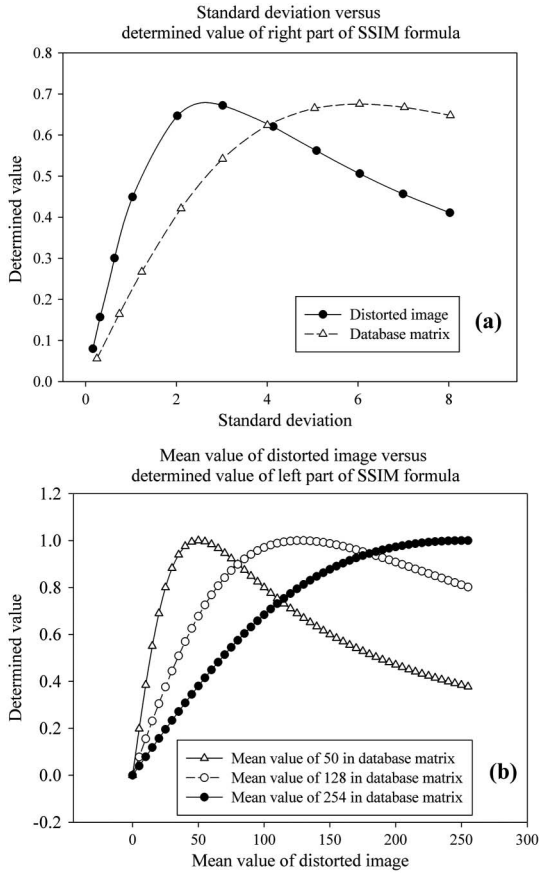

Fig. 7. Summary of the variables varying with the determined value of SSIM formula (Eq. 1). (a) Standard deviation versus the value of the right part of SSIM formula. (b) Mean value versus the value of the left part of SSIM formula.

be determined by the two parts multiplied. Therefore, the maximal SSIM value can be determined in the differential equation of SSIM and the available mean value of the database matrix also can be determined in the differential equation.

The maximum range of the gray level in the database matrix is determined, in which the differential equation of SSIM and the other parameters, $\mu_r, \mu_t, \sigma_r^2, \sigma_t^2$, and σ_{rt}, are denoted as follows:

$$\mu_r = \frac{1}{N^2}\sum_{i,j=1}^{N} \mathrm{Gray}_r(i,j), \tag{7}$$

$$\mu_t = \frac{1}{N^2}\sum_{i,j=1}^{N} \mathrm{Gray}_t(i,j), \tag{8}$$

$$\sigma_t^2 = \frac{1}{(N-1)^2}\sum_{i,j=1}^{N} [\mathrm{Gray}_t(i,j) - \mu_t]^2, \tag{9}$$

$$\sigma_r^2 = \frac{1}{(N-1)^2}\sum_{i,j=1}^{N} [\mathrm{Gray}_r(i,j) - \mu_r]^2, \tag{10}$$

$$\sigma_{\mathrm{rt}} = \frac{1}{N-1}\sum_{i,j=1}^{N} [\mathrm{Gray}_r(i,j) - \mu_r] \times [\mathrm{Gray}_t(i,j) - \mu_t], \tag{11}$$

$$\begin{aligned}
\frac{\partial \mathrm{SSIM}}{\partial \mu_r} &= \frac{B'A - A'B}{[(\mu_t^2 + \mu_r^2 + C_1)(\sigma_t^2 + \sigma_r^2 + C_2)]^2}, \\
A &= (2\mu_t\mu_r + C_1)(2\sigma_{tr} + C_2), \\
B &= (\mu_t^2 + \mu_r^2 + C_1)(\sigma_t^2 + \sigma_r^2 + C_2), \\
A' &= 2\mu_t(2\sigma_{\mathrm{tr}} + C_2) + (2\mu_t\mu_r + C_1) \\
&\quad \times \left[\frac{2}{N-1}\sum_{x,y=1}^{N} -(\mathrm{Gray}_t(x,y) - \mu_t)\right], \\
B' &= 2\mu_r(\sigma_t^2 + \sigma_r^2 + C_2) + (\mu_t^2 + \mu_r^2 + C_1) \\
&\quad \times \left[\frac{2}{(N-1)^2}\sum_{x,y=1}^{N} -(\mathrm{Gray}_r(x,y) - \mu_r)\right],
\end{aligned} \tag{12}$$

where N denotes the number of pixels, $\mathrm{Gray}_r(i,j)$, and $\mathrm{Gray}_t(i,j)$ denotes the gray levels of the r and t images.

In Eq. (12), the maximum differential value of μ_r is difficult to be solved, explaining the use of the numerical method to determine the maximum differential value. Additionally, the gray level of the black windows of the database matrix is changed from 0 to 200 to determine the working range of the fiducial points finding with the SSIM method and the gray level of the white windows in the database matrix is fixed as 255.

3. Experiments

All experiments are conducted with a coaxial HDSS, as schematically depicted in Fig. 8. In contrast to GLWM (center), the proposed algorithm is implemented in three cases. In Case 1, L4 symbolizes a Fourier lens, providing a high SNR as well as less aberration, while in Case 2, a usual lens, rather than the Fourier lens, is employed to enhance the system aberration effect and render a degraded SNR, for the reason that the magnification here is superior to that in Case 1 in the context of constant exposure time and laser power. Finally, in Case 3, translating the SLM by the displacements of −0.1 mm to 0.1 mm, the system is made operated in a low SNR circumstance.

Adopting the previous research data [12], there are a total of 2.16×10^6 bits of raw data, coded with a Reed Solomon code (31, 25, and 3), 1024 bits per page, each bit covering 4×4 pixels onto a SLM with a pixel pitch of 19 μm. With the Fourier lens with 375 mm focal length employed in Case 1, the system exhibits a magnification of roughly 2.7, with a bit covering 18×18 pixels onto an image sensor with a pixel pitch of 12 μm, while employing the usual lens with 500 mm focal length, Cases 2 and 3 demonstrate a magnification of 3.7 or so, with a bit covering 23×23 pixels on the image sensor. The SLM of Case 3 is shifted from −0.1 to 0.1 mm, except at 0 mm, with a displacement 0.05 mm and the SLM position of Case 2 is at 0 mm.

Database matrices of sizes 18×18 and 24×24 pixels are used to sweep the checkerboard images, respectively, in various cases, with gray levels of 50 and 255 corresponding to black and white, respectively. The size of the database matrices is determined by the maximal even integer, which is more than or equal to the size of a bit in the checkerboard image. In the noise-free system, the determined size is the minimal size to completely surround each center in the 2×2 bits of the checkerboard image. As the database matrices moving out the correct position (position 2 in Fig. 5) in the checkerboard image, the SSIM value

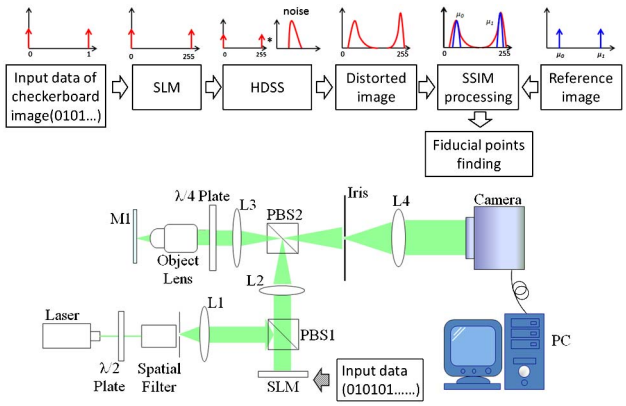

Fig. 8. (Color online) Sketch of HDSS and a block diagram of the fiducial point finding.

would be decreased and lower than the value in the correct position. For conducting a sweep trial, an arbitrary choice of the checkerboard images is made, or two images, alternate conversely in black and white, are selected, in which the fiducial points are identified successfully, as expected. The swept image, below normalized background noise of 0.1 (approximately gray level of 25), is subsequently treated as the noise, set to 0. Then, using matrices of sizes 19×19 and 25×25 pixels to scan the swept images, respectively, the fiducial points are hence identified, if the maximum value is situated at the matrix center, aggregated, and then applied to subsequent images. The size of the swept matrices cannot be large to surround each center in the 2×2 bits of the checkerboard image, owing to the swept matrices filtering the fiducial point as maximal SSIM value in a bit window. Therefore, the size of the swept matrices is determined by the minimal odd integer, which is under the size of a bit in the checkerboard image. In Cases 1 and 2, the locations of fiducial points are reached by first performing GLWM and the SSIM method on the sensed corresponding image. Meanwhile, in Case 3, the task is done by the fiducial points derived from Case 2. Therefore, matrices around the fiducial points of sizes 9×9, 11×11, 13×13, 15×15, 17×17, 19×19, and 21×21 pixels are thus extracted and averaged to graph the histograms. By using Eqs. (2) and (3), BER as well as SNR is evaluated; in addition, both approaches are compared in terms of accuracy. An average matrix of large size covers a large window of the image sensed, leading to a low BER and fiducial points staying toward the window center. Furthermore, the solution for optimized BER is found in case of the raw data with minimal or no errors.

4. Results and Discussion

Figure 9 displays an image commonly received in three cases and the SNRs of three cases are summarized in Table 1. This figure reveals that Case 1, a high SNR system, exhibits an extremely sharp window border, low aberration effect, and satisfactory BER with arbitrary alignment methods, yet at the cost of expensive optical components. However, since a normal lens is used in Cases 2 and 3, the image quality is degraded due to the effects of aberration and noise. Especially in Case 3, the window border turns blurry owing to the shift effect.

Figures 10 and 11 summarize the numerical results of the working range of the fiducial points in Cases 1 and 2, respectively. The numerical results determined from Eq. (12), the database matrices sweeps over the distorted checkerboard image following SSIM operation, and the database matrices of sizes 13×13 and 19×19 pixels are selected as the minimal BER determined in Cases 1 and 2, respectively. Then, the differential values, on the fiducial points are collected to plot Figs. 10 and 11. The curve is separated into two parts: positive correlation in the top part and negative correlation in the bottom

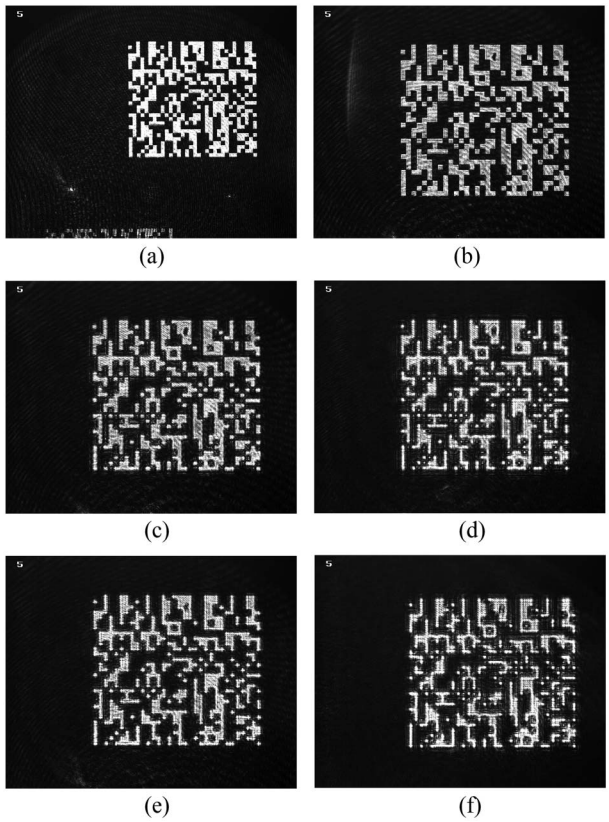

Fig. 9. Image commonly received in three cases, that is, (a) Flens, (b) Nlens, (c) −0.05 mm shifting, (d) −0.1 mm shifting, (e) +0.05 mm shifting, (f) +0.1 mm shifting in descending order.

part. For example, since database matrix 1 sweeps over the checkerboard image, parts of the fiducial points have a negative correlation as the positions of fiducial points in the black windows. The negative correlation means that the two images are not similar to each other in the luminance, contrast, or structure and determined SSIM index is negative, and vice versa. In Table 1, the SNR of Case 1 is higher than Case 2, explaining why Case 1 has fewer aberrations effect to achieve the flatness curve of the mean value in Fig. 9. The approximate working ranges of SSIM method can be determined from the positions of the turning points in the top envelope of the positive correlation part. Because the positions of the turning points of the fiducial points are dissimilar to each other, each gray level in the approximate working range is utilized to determine and verify the fiducial points correctly in the fiducial points finding. Eventually, the working range is redefined by the

Table 1. Summary of the SNR in All Cases

Case	SNR
Case 1 (Flens)	~20
Case 2 (Nlens)	~10
Case 3 with shifting +0.05 mm (Nlens)	~8.5
Case 3 with shifting −0.05 mm (Nlens)	~6.8
Case 3 with shifting −0.1 mm (Nlens)	~5.5

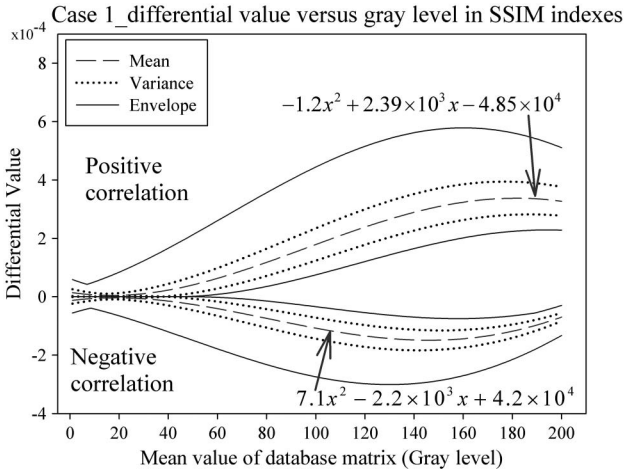

Fig. 10. Plot of differential value versus gray level for a database matrix sweeping over the checkerboard image in Case 1.

gray levels, which can determine the fiducial points correctly. In the GLWM method, the working range can be determined by the thresholds varying as the fiducial points determined correctly. Therefore, the working ranges of the threshold in Cases 1 and 2 by using GLWM are 11 (gray level of threshold from 154 to 165) and 31 (gray level of threshold from 124 to 155), respectively, and the working ranges of the gray level of the database matrices by using SSIM method in Cases 1 and 2 are increased to 100 and 120, respectively. The wider range of the gray level by using SSIM method is owing to the SSIM index decreasing quickly as the database matrix sweeps over a nonuniform or imperfect image. The larger working range in Case 2 is owing to the slight overexposure in the Case 1. However, the SSIM method supports a wider threshold range of gray level than the GLWM does.

According to Fig. 12, Case 1 is of a minimum BER of 3.42×10^{-47} redundant noise interference is filtered using a higher oversampling ratio [15–16]. By using the SSIM method, the fiducial points located at the window centers are more accurate than GLWM.

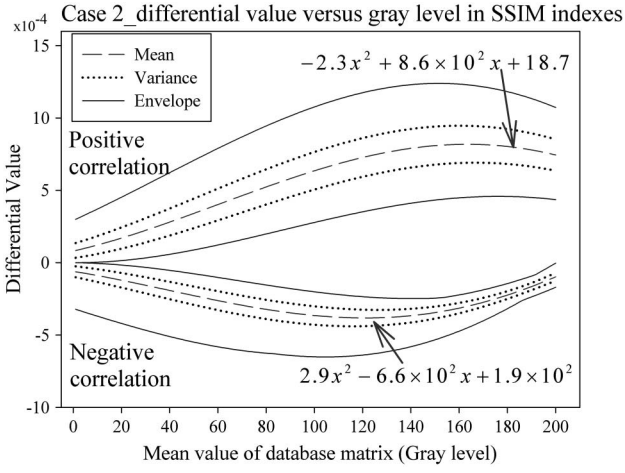

Fig. 11. Plot of differential value versus gray level for a database matrix sweeping over the checkerboard image in Case 2.

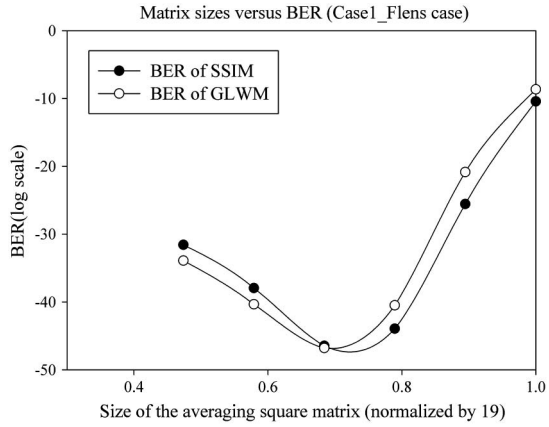

Fig. 12. Comparison result of matrix size versus BER in Case 1.

Thus, an oversized matrix can still cover the corresponding window area. Compared with GLWM, a slightly higher level of BER occurs in the SSIM method, owing to IPI as well as a slight amount of dust, when the matrix size is below 13×13 pixels. With a larger size of the matrix, a lower level of BER is as expected yielded by the SSIM method. However, an averaging matrix with larger sized reducing IPI in the white windows, the BER of the SSIM method (2.71×10^{-26}) provides 5 orders lower

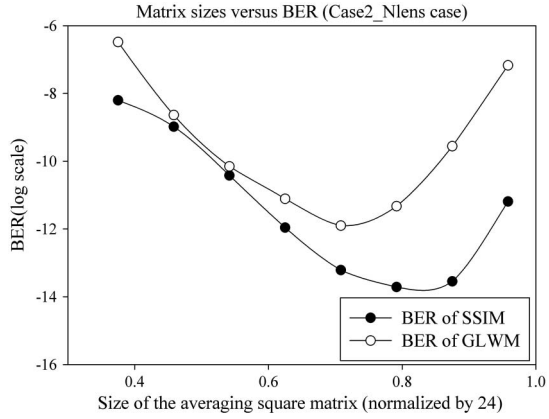

Fig. 13. Comparison result of matrix size versus BER in Case 2.

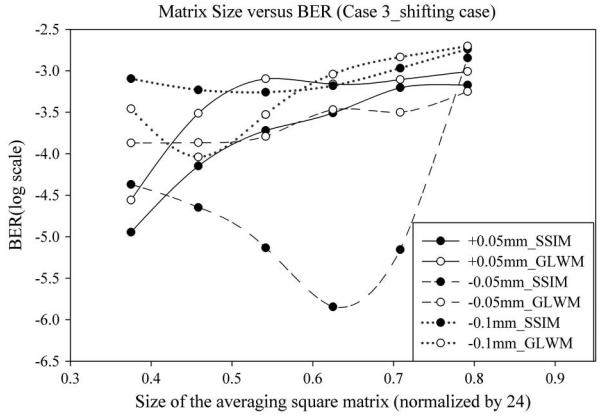

Fig. 14. Comparison result of matrix size versus BER in Case 3.

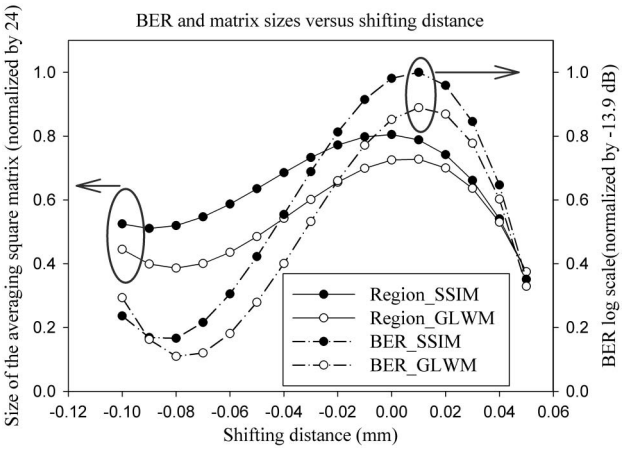

Fig. 15. Summary of shifting distance effects in HDSS.

than GLWM (1.43×10^{-21}) in the 17×17 pixel matrix size. According to Fig. 13, the comparison results in Case 2 indicate that the SSIM method performs better than GLWM at most of the matrix sizes while the lower SNR does. The fiducial points located by the SSIM method are closer the windows center than GLWM. Thus, the system has a satisfactory BER 2.85×10^{-14}, and the BER provides 4 orders lower than GLWM (2.77×10^{-10}) in the 21×21 pixel matrix size. In the two cases, the matrix size accounts for $0.76\sim0.8$ of the pixels by one bit on the received checkerboard image, the lowest level of BER obtained, when the fiducial points have an accurate alignment. Figure 14 summarizes the comparison results of Case 3, a defocus system, which bends the window border outward.

The SSIM method also apparently demonstrates a lower BER than GLWM when using an arbitrary size of matrix, thus, confirming that the proposed method is the most effective means of seeking the center location of windows. In summing up Cases 2 and 3, the shifting distance versus the lowest BER and the matrix size of Cases 2 and 3 are fitted and presented in Fig. 15. An ideal case is one in which the peak locations of the BER and matrix size overlap. However, a displacement between the peaks of the lowest BER and the matrix size is due to the aberration balanced by defocus [17].

5. Conclusions

This work compares GLWM and the SSIM method in three cases in terms of the center location. Consequently, the SSIM method is a more accurate means of locating the window center, especially in the context of defocus, ultimately reaching a low level of BER as well. Therefore, inexpensive optical elements in HDSS can be utilized to decrease system costs as the SSIM method. There are two problems involving the SSIM method, one in which the windows in the checkerboard image edge cannot fully compare with the database matrix such as to derive a lower SSIM value, and the other one in which SSIM method is five times the calculation time of GLWM method (SSIM: 183.5 s and GLWM: 35.8 s). Characterized by a human model, SSIM is adopted to provide two advantages in which the problem of multiple fiducial points caused by a single threshold is subsequently removed. Additionally, more factors, i.e., the image contrast and structure, are both considered. Restated, the center can still be precisely located, even in the case of an aberration, as caused from the checkerboard image received. Furthermore, the centering task can still be fulfilled by a checkerboard image (as mentioned earlier) by the SSIM method, even though either of the two images is damaged or unidentified. We conclude that the proposed SSIM method, developed based on the SSIM algorithm, has a superior centering accuracy, more image parameters considered, as well as other advantages, making it more applicable to a HDSS than to GLWM.

This paper is particularly supported by "Aim for the Top University Plan" of the National Chiao Tung University and the Ministry of Education, Taiwan, Technology Development Program for Academia in Taiwan, the National Science Council of Taiwan, and Delta Electronics Incorporation. The authors want to thank them for providing experimental assistance and related information. Ted Knoy is appreciated for his editorial assistance.

References

1. G. W. Burr, W. C. Chou, M. A. Neifeld, H. Coufal, J. A. Hoffnagle, and C. M. Jefferson, "Experimental evaluation of user capacity in holographic data-storage systems," Appl. Opt. **37**, 5431–5443 (1998).
2. S. S. Orlov, W. Phillips, E. Bjornson, Y. Takashima, P. Sundaram, L. Hesselink, R. Okas, D. Kwan, and R. Snyder, "High-transfer-rate high-capacity holographic disk data-storage system," Appl. Opt. **43**, 4902–4914 (2004).
3. D. Park and J. Lee, "Holographic data storage channel model with intensity factor," IEEE Trans. Magn. **45**, 2268–2271 (2009).
4. H. Horimai and X. D. Tan, "Holographic information storage system: Today and future," IEEE Trans. Magn. **43**, 943–947 (2007).
5. G. W. Burr, H. Coufal, R. K. Grygier, J. A. Hoffnagle, and C. M. Jefferson, "Noise reduction of page-oriented data storage by inverse filtering during recording," Opt. Lett. **23**, 289–291 (1998).
6. G. W. Burr and T. Weiss, "Compensation for pixel misregistration in volume holographic data storage," Opt. Lett. **26**, 542–544 (2001).
7. G. W. Burr, "Holographic data storage with arbitrarily misaligned data pages," Opt. Lett. **27**, 542–544 (2002).
8. J. F. Heanue, K. Gurkan, and L. Hesselink, "Signal detection for page-access optical memories with intersymbol interference," Appl. Opt. **35**, 2431–2438 (1996).
9. M. A. Neifeld and M. McDonald, "Technique for controlling cross-talk noise in volume holography," Opt. Lett. **21**, 1298–1300 (1996).
10. W. C. Chou and M. A. Neifeld, "Interleaving and error correction in volume holographic memory systems," Appl. Opt. **37**, 6951–6968 (1998).
11. M. Ayres, A. Hoskins, and K. Curtis, "Image oversampling for page-oriented optical data storage," Appl. Opt. **45**, 2459–2464 (2006).
12. M. Ou-Yang and Y. T. Chen, "A gray level weighting method to reduce optical aberration effect in holographic data storage system," IEEE Trans. Magn. **47**, 546–550 (2011).
13. Z. Wang, A. C. Bovik, H. R. Sheikh, and E. P. Simoncelli, "Image quality assessment: from error visibility to structural similarity," IEEE Trans. Image Process. **13**, 600–612 (2004).

14. Z. Wang and A. C. Bovik, "Mean squared error: love it or leave it? A new look at signal fidelity measures," IEEE Signal Process. Mag. **26**, 98–117 (2009).
15. M. A. Neifeld and W. C. Chou, "Information theoretic limits to the capacity of volume holographic optical memory," Appl. Opt. **36**, 514–517 (1997).
16. G. P. Nordin and P. Asthana, "Effects of cross-talk on fidelity in page-oriented volume holographic optical-data storage," Opt. Lett. **18**, 1553–1557 (1993).
17. W. C. Chou and M. A. Neifeld, "Interleaving and error correction in volume holographic memory systems," Appl. Opt. **37**, 6951–6968 (1998).